applied sciences

MDPI

Article

Energy Absorption Characteristics and Parameter Optimization of Anti-Climb Energy-Absorbing Devices for Subway Vehicles under Impact Loads

Yuru Li [1,2,3,*], Hao Zhang [1], Junke Xie [1], Shoune Xiao [2], Tao Zhu [2], Gangjian Zhou [1] and Liyou Xu [1]

[1] College of Vehicle and Traffic Engineering, Henan University of Science and Technolgy, Luoyang 471003, China; 210321030347@stu.haust.edu.cn (H.Z.); 9943597@haust.edu.cn (J.X.); 230320030367@stu.haust.edu.cn (G.Z.); xlyou@haust.edu.cn (L.X.)
[2] State Key Laboratory of Rail Transit Vehicle System, Southwest Jiaotong University, Chengdu 610031, China; snxiao@swjtu.edu.cn (S.X.); zhutao034@swjtu.edu.cn (T.Z.)
[3] CRRC Qiqihar Rolling Stock Co., Ltd., Qiqihaer 161000, China
* Correspondence: lyr@haust.edu.cn

Abstract: To further enhance the crashworthiness of subway vehicle anti-climb energy-absorbing devices, this paper proposes a novel collapsible structure, which is embedded with honeycomb aluminum blocks and consists of an inner and outer double-layer square tube. An impact finite element model of the subway vehicle's anti-climb energy-absorbing device was established using LS-DYNA (v.17.2). The effects of the connecting diaphragm thickness, the inner and outer tube thicknesses of the thin-walled tubes, and the yield strength of the honeycomb aluminum on the energy absorption and impact force of the anti-climb energy-absorbing device were investigated. The results indicate that changes in the inner and outer tube thicknesses of the thin-walled tubes significantly affect the energy absorption and impact force of the anti-climb energy-absorbing device. However, changes in the connecting diaphragm thickness only increase the maximum energy absorption by up to 7.5% but have a significant impact on the maximum peak force. It was also found that the difference in energy absorption due to changes in the yield strength of the honeycomb aluminum is only 3.6%, suggesting that the yield strength of the honeycomb aluminum and the connecting diaphragm thickness have a limited influence on the crashworthiness design of the anti-climb energy-absorbing device. Furthermore, a multi-objective surrogate model characterizing the specific energy absorption and maximum peak force was established for the aforementioned four influential parameters using the response surface method. The model was then optimized using a genetic algorithm, resulting in optimal parameters that increased the energy absorption and specific energy absorption by 27.3% and 13.8%, respectively, compared to the original values, leading to a significant improvement in crashworthiness. The findings provide valuable references for and insights into the crashworthiness design and optimization of subway vehicles' anti-climb energy-absorbing devices.

Keywords: anti-climb energy-absorbing devices; crashworthiness; energy absorption characteristics; surrogate model; optimization

check for updates

Citation: Li, Y.; Zhang, H.; Xie, J.; Xiao, S.; Zhu, T.; Zhou, G.; Xu, L. Energy Absorption Characteristics and Parameter Optimization of Anti-Climb Energy-Absorbing Devices for Subway Vehicles under Impact Loads. *Appl. Sci.* **2024**, *14*, 5203. https://doi.org/10.3390/app14125203

Academic Editor: Muhammad Junaid Munir

Received: 15 May 2024
Revised: 11 June 2024
Accepted: 13 June 2024
Published: 14 June 2024

Copyright: © 2024 by the authors. Licensee MDPI, Basel, Switzerland. This article is an open access article distributed under the terms and conditions of the Creative Commons Attribution (CC BY) license (https://creativecommons.org/licenses/by/4.0/).

1. Introduction

The anti-climb energy-absorbing devices at the ends of subway vehicles play a crucial role in preventing climbing during collisions and reducing structural damage to the vehicle body. They are one of the key components of passive safety protection for rail vehicles. During a collision or rear-end impact, the dynamic impact response is complex, with a high likelihood of longitudinal compression, body buckling, overturning, and arching climbing phenomena. Studies have shown that end anti-climb energy-absorbing devices can effectively inhibit vehicle climbing, reduce harm to passengers and crew, and minimize property damage [1]. Anti-climb energy-absorbing devices are categorized based on their

energy-absorbing modes into cutting, crushing, and expanding types. Crushing-type anti-climb energy-absorbing devices filled with honeycomb structures have been widely used in rail trains due to their advantages of being lightweight, having a high level of specific energy absorption, and having controllable deformation.

Current research on anti-climb energy-absorbing devices still has some shortcomings. For instance, crushing-type anti-climb energy-absorbing devices are prone to axial instability under offset conditions, which significantly reduces their energy absorption effectiveness. Cutting-type anti-climb energy-absorbing devices have drawbacks such as high material requirements and low utilization rates. Expanding-type anti-climb energy-absorbing devices suffer from low impedance force levels and small energy absorption capacities [2]. To address the issues with anti-climb energy-absorbing devices, structural optimization is employed and new materials are applied to achieve orderly and controllable compression deformation, enhancing the energy absorption efficiency and increasing the energy absorption capacity. Gao et al. [3] conducted experimental research on a new type of energy absorber, indicating that the cutting deformation mode of aluminum tubes is more stable than that of steel pipes, with the axial cutting force increasing as the strength of the crushed tube material and the depth of the cutting increase. Jiang Shihong [4] designed a honeycomb anti-climb device for rail vehicles and performed a simulation analysis and experimental verification of the energy-absorbing performance of the anti-climb energy-absorbing device. The simulation results were highly consistent with the experimental results, and the designed anti-climb device met the requirements for energy absorption and anti-climbing. Peng et al. [5] studied the crashworthiness characteristics of the composite energy-absorbing structure of subway vehicle anti-climb energy-absorbing devices through experiments and numerical simulations, analyzing the impact of tube thickness and honeycomb material parameters on the structural energy-absorbing performance. Their study showed that the honeycomb thickness significantly affects the initial peak force and average collision force. Gao et al. [6] conducted crashworthiness tests of a retracted tube anti-climb energy-absorbing device on a component-level collision test bench, demonstrating that the proposed retracted tube anti-climb energy-absorbing device improved the train's crashworthiness in eccentric and inclined collision scenarios. Filling the interior of the anti-climb energy-absorbing device with foamed aluminum not only effectively increases the specific energy absorption but also helps control the deformation mode of the anti-climb energy-absorbing device [7]. Studies have shown that foamed aluminum-filled honeycomb cells play an important role in mitigating structural deformation caused by lateral impacts [8,9], leading to an increasing application of this structure in the design of energy-absorbing devices.

In the context of crashworthiness optimization for anti-climb energy-absorbing devices, the optimization of crashworthiness often involves the establishment of polynomial models for energy absorption indicators using surrogate models, followed by the application of optimization algorithms for structural crashworthiness design [10]. Ihsan et al. [11] used Taguchi's robust parameter method to estimate the optimum configuration and found the most influential parameters are the anti-climber material (29.79%) for the system's crash energy absorption performance and teeth thickness (50.26%) for the crash box deformation performance. Chen et al. [12] utilized the response surface method to study the influence of the factors of height and inclination angle of anti-climb teeth on the anti-climbing capability of a device. Djamaluddin et al. [13] conducted a finite element analysis and optimization design research on the crashworthiness of foam-filled double circular tubes for energy absorption optimization with aluminum honeycomb-filled thin-walled tubes. Yildiz et al. [14] applied particle swarm optimization algorithms in the optimization of subway vehicle anti-climb energy-absorbing devices, conducting a multi-objective optimization analysis of the front-end energy-absorbing structure and honeycomb-filled thin-walled structure of subway vehicles. This led to the identification of the Pareto front of specific energy absorption, achieving the ideal values for optimal specific energy absorption and initial peak force. Meanwhile, Yin et al. [15] employed a multi-objective optimization approach targeting both

the maximum specific energy absorption and maximum impact force, realizing the crashworthiness optimization of functionally graded foam-filled tubes and uniform foam-filled tubes and obtaining a series of Pareto optimal solutions. Marzbanrad et al. [16] studied the crushing behavior of thin-walled aluminum tubes under axial impact loads and conducted a multi-objective optimization of five crushing parameters of circular aluminum tubes under axial compression loads using the linear weighting method, based on different priorities. In a modular scenario optimization, Zheng et al. [17] established a collaborative optimization platform for the design of collision energy-absorbing devices (anti-climb energy-absorbing devices) of high-speed trains using a modular modeling system, achieving an optimized scenario design for the energy-absorbing devices. Li et al. [18,19] combined finite element and neural network algorithms to study the structural optimization and energy absorption characteristic predictions of anti-climb energy-absorbing devices, providing an important method for conducting efficient computational analyses of these devices.

To further enhance the energy absorption efficiency and crashworthiness of anti-climb energy-absorbing devices, this paper proposes a novel anti-climb energy-absorbing device, which is composed of inner and outer thin-walled square tubes and honeycomb structures that absorb energy together. This study investigates the impact of the thin-walled tubes, connecting diaphragm thickness, and the yield strength of the aluminum honeycomb on the energy absorption characteristics and impact force of the anti-climb energy-absorbing device to establish their patterns of influence. By using the design of experiments (DOE) for the anti-climb energy-absorbing device, a multi-objective surrogate model characterizing its specific energy absorption and peak force is established. Finally, a multi-island genetic algorithm is employed to optimize the model and obtain the optimal structural parameters. Through the optimization analysis of the proposed novel anti-climb energy-absorbing device, the energy absorption performance of the device is improved, which is of significant importance for enhancing the crashworthiness of rail vehicles in collision accidents.

2. Model Establishment

2.1. Finite Element Model

The anti-climb device mainly consists of several components, including anti-climb teeth, an anti-climb tooth mounting plate, an outer tube, a honeycomb structure, a connecting diaphragm, a mounting plate, guide beams, and an inner tube. The finite element model of the device is depicted in Figure 1. The active vehicle impacts the passive vehicle at a certain impact velocity, and the subway car is organized in 6 groups. The anti-climbing energy absorption devices are respectively installed on the front end of the subway vehicles. The guide beams provide bending stiffness to the structure of the anti-climb energy-absorbing device and serve a guiding function. They are welded to the front anti-climb teeth and, during the collision process, are designed to retract through the mounting plate's aperture without undergoing plastic deformation. The aluminum honeycomb energy-absorbing blocks and the inner and outer thin-walled tubes constitute the primary energy-absorbing structures. These energy-absorbing blocks, connecting diaphragms, and guide beams are housed within a metallic thin-walled outer tube, which is connected at its front and rear ends to the anti-climb tooth mounting plate and the mounting plate, respectively. The anti-climb device employs a multi-stage honeycomb series structure, in which different honeycombs are separated by connecting diaphragms, allowing for a more orderly and controllable deformation while the honeycomb is crushed. An induction groove is set at the front end of the outer tube to reduce the initial peak force. During a collision, the thin-walled shell structure will first undergo folding and crushing, followed by an orderly folding deformation. The material parameters of each component of the anti-climb device are presented in Table 1.

Our finite element model of the anti-climb energy-absorbing device is primarily composed of shell elements and solid elements. The connections are predominantly simulated through rigid connections that mimic the welding between components. The model consists

of a total of 329,535 elements, with 125,722 of these being shell elements and 203,813 being solid elements. The aluminum honeycomb material is represented using MATL26 [20] and the other materials using MATL3. In terms of contact settings, the model predominantly features automatic surface-to-surface contact and automatic single-surface contact. The dynamic and static friction coefficients are set to 0.2 and 0.15, respectively. The types of finite element model units and the specific contact relationships are illustrated in Figure 2.

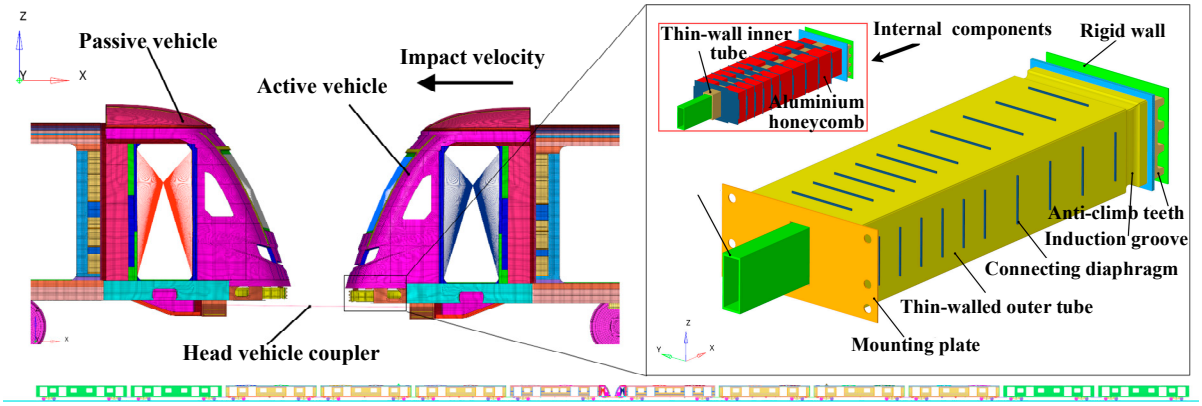


Figure 1. Composition of the anti-climb energy-absorbing device.

Table 1. Material properties.

Component	Material	Density/(kg/m^3)	Elastic Modulus/GPa	Poisson's Ratio	Yield Strength/MPa
Anti-Climb Teeth	#45 steel	7800	210	0.3	350
Anti-Climb Teeth Installation Plate	Aluminum alloy6060	2700	70	0.3	180
Thin-Walled Outer Tube	Aluminum alloy6060	2700	70	0.3	180
Thin-Walled Inner Tube	Aluminum alloy6060	2700	70	0.3	180
Aluminum Honeycomb	Aluminum alloy	60.3	69	0.3	/
Partition Panel	Aluminum alloy6060	2700	70	0.3	180
Mounting Plate	Aluminum alloy6060	2700	70	0.3	180
Guiding Beam	#45 steel	7800	210	0.3	350

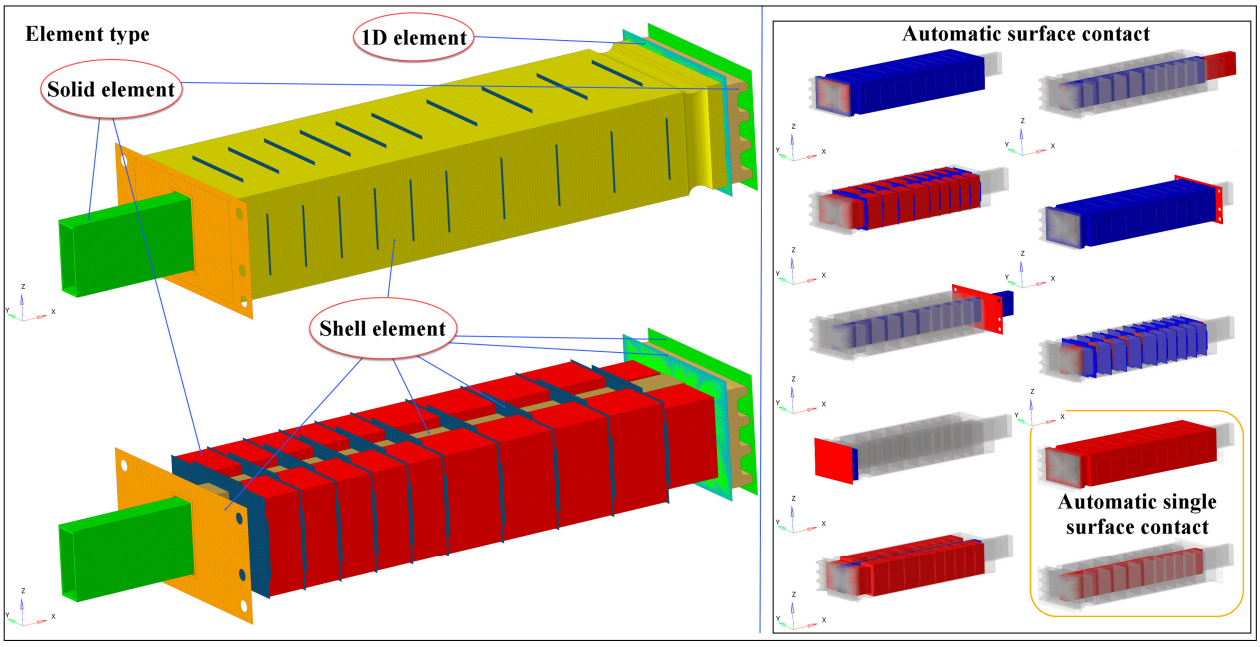


Figure 2. Element types and contact relationships of the anti-climb energy-absorbing device.

2.2. Collision Scenario of the Anti-Climb Energy-Absorbing Device

Self-contact is set for each component of the anti-climb device, including the internal partition walls, honeycomb structures, and guiding beams with the external thin-walled shell, which have surface-to-surface contact. The front anti-climb teeth also have surface-to-surface contact with a rigid wall. The rigid wall is fixed, and a certain distance is maintained from the anti-climb device. To adhere to the European Union's EN 15227 standard [21] for train vehicle collision design, a moving rigid wall is used to perform the crushing. The speed of the rigid wall is set at 25 km/h, impacting the anti-climb energy-absorbing device at a constant speed. An effective compression distance of 550 mm is designed, and its position and direction of velocity are depicted in Figure 3.

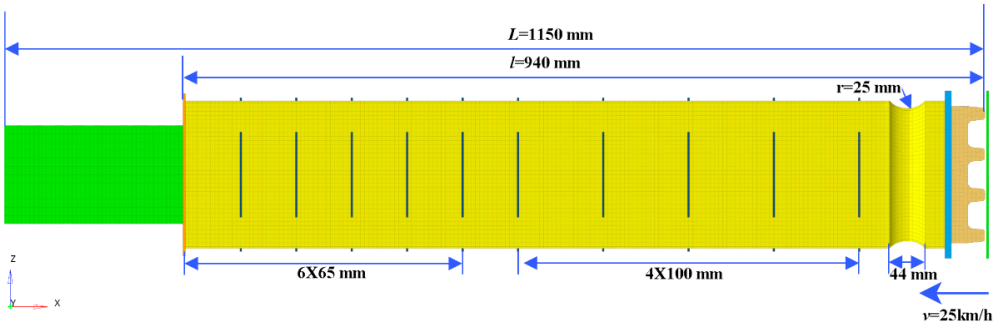


Figure 3. Impact parameters of the anti-climb energy-absorbing device.

3. Energy Absorption Characteristics

Evaluation Criteria

During the collision process, the anti-climb energy-absorbing device primarily absorbs energy through the plastic crushing deformation of the aluminum honeycomb and the inner and outer thin-walled tubes. In addition to considering the total energy absorbed by the anti-climb device, it is also important to avoid excessively high collision peak forces, as these can lead to high-impact accelerations that may cause injury to passengers inside the vehicle. Therefore, this paper employs the specific energy absorption and the peak crush force to evaluate the energy absorption effectiveness.

(1) Specific Energy Absorption

The specific energy absorption (*SEA*) represents the energy that a unit mass of the energy-absorbing structure can absorb. The higher the specific energy absorption, the better the energy absorption effect of the structure. To enhance the crashworthiness of the structure and meet the design requirements specifying the device should be lightweight, the specific energy absorption of the energy-absorbing structure should be maximized.

Q represents the energy absorbed by the energy-absorbing structure during its buffering deformation and is defined as follows:

$$Q = \int_0^l F(l)dl \tag{1}$$

In the formula, $F(l)$ represents the relationship between the impact force and the displacement function, and l is the effective crushing deformation displacement.

SEA is an important index of crashworthiness, representing the capacity for energy absorption per unit mass, and it directly reflects the quality of the energy-absorbing structure design. The formula is as follows:

$$SEA = \frac{Q}{M} \tag{2}$$

In the formula, M represents the mass of the anti-climb energy-absorbing device.

(2) Peak Force

Peak force F refers to the maximum impact force during the energy absorption process, which typically occurs in the initial stage. The magnitude of the peak force has a significant impact on the structural safety of the train and the comfort of the passengers, and it is desirable for it to be as close as possible to the mean force. The peak force is an important metric for measuring the energy absorption capacity of an energy-absorbing device during a collision. A smaller peak force implies that the collision energy can be more effectively absorbed and dispersed, thereby reducing the impact force transmitted to the main body of the vehicle and its occupants.

Mean force F_M is the average value of the impact force over a specified crushing displacement. Its formula is as follows:

$$F_M = \frac{Q}{l} \tag{3}$$

4. Structural Crashworthiness

4.1. Influence of Connecting Diaphragm Thickness

Connecting diaphragms can constrain bending modes, and connecting diaphragms are capable of constraining the buckling modes, allowing the energy-absorbing structure to undergo sequential progressive buckling, thereby enhancing its energy absorption capacity. Due to the limited size of individual aluminum honeycomb cells, they cannot meet the substantial energy absorption requirements of subway vehicles during a collision. Moreover, increasing the size of a single honeycomb cell can easily lead to instability during the collision, resulting in a less-than-ideal deformation pattern. Therefore, multiple aluminum honeycomb cells are used in series, with the spacing between honeycombs as shown in Figure 3, and connecting diaphragms are inserted in between them. This combined arrangement significantly increases the energy absorption capability of the honeycombs. The role of the connecting diaphragms is to prevent adjacent honeycomb blocks from interlocking, which could deteriorate the energy absorption effect, ensuring a more stable and orderly deformation process. Consequently, the thickness of the connecting diaphragms has a significant impact on the energy absorption outcomes of the entire aluminum honeycomb anti-climb device.

Variable thicknesses of the connecting diaphragms, denoted as t1, are selected with values of 2, 3, 4, 5, and 6 mm. The impact force and energy absorption are calculated for each connecting diaphragm thickness. Figure 4 presents the collision force–displacement curves and energy absorption–displacement curves for different connecting diaphragm thicknesses.

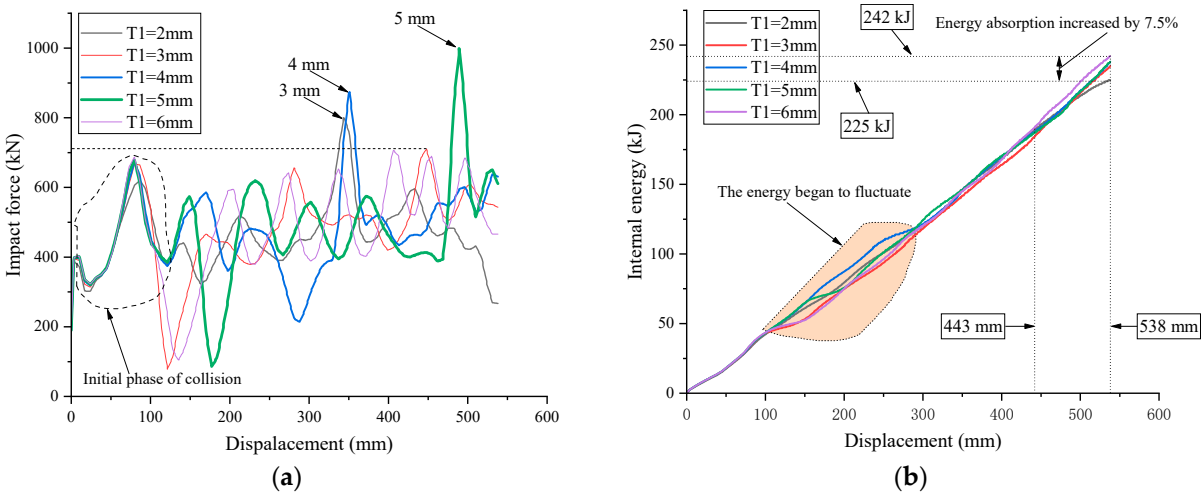


Figure 4. (**a**) Collision force–displacement curves for different connecting diaphragm thicknesses; (**b**) Energy absorption–displacement curves for different connecting diaphragm thicknesses.

From Figure 4a, it can be observed that different connecting diaphragm thicknesses have a significant impact on the impact force of the anti-climb energy-absorbing device, while having a smaller effect on the initial peak force. In the initial stage, except for the connecting diaphragm with a thickness of 2 mm, which shows a distinct difference, the impact force and initial peak force for the other thickness parameters remain consistent. This indicates that the connecting diaphragm thickness does not significantly affect the initial peak force of the anti-climb energy-absorbing device. However, after the initial stage, it is found that different connecting diaphragm thicknesses have a more pronounced effect on the maximum impact force peak value. Especially for the 5 mm thickness, the maximum peak force approaches 1000 kN, which is significantly higher than the initial peak force, and the maximum peak force also increases with the increase in connecting diaphragm thickness. Therefore, when designing the partition walls for the anti-climb energy-absorbing device, it is necessary to consider the impact of the connecting diaphragm on the peak force, aiming to reduce the connecting diaphragm thickness as much as possible while ensuring the energy absorption effect of the device.

Figure 4b shows that in the initial stage, the energy absorption does not change with the connecting diaphragm thickness and has a minor effect on energy absorption. As the compression displacement increases, there is a certain fluctuation in the energy absorption. When the connecting diaphragm thickness is 4 mm, the energy absorption is the greatest. After the compression displacement exceeds 443 mm, the anti-climb energy-absorbing device with a 5 mm connecting diaphragm thickness has the highest energy absorption. At a compression displacement of 538 mm, there is a trend that the energy absorption increases with the increase in connecting diaphragm thickness, with the energy absorption of the 6 mm connecting diaphragm being 7.5% higher than that of the 3 mm partition wall. This suggests that the connecting diaphragm thickness will have a significant impact on energy absorption when the compression displacement is relatively large. This may be due to the deformation of the connecting diaphragm when the crushing displacement of the anti-climb energy-absorbing device reaches a certain value, leading to a change in energy absorption.

4.2. Influence of Thin-Walled Outer Tube Thickness

When subjected to impact, the anti-climb energy-absorbing device can undergo an orderly plastic deformation designed to absorb the initial kinetic energy, reduce the impact on the vehicle structure, and enhance the vehicle's safety. To investigate the effects of the thin-walled tube thickness on the energy absorption characteristics and collision force, the thickness $t2$ of the thin-walled outer tube is set to 2, 3, 4, 5, and 6 mm, respectively, to obtain the crashworthiness performance of the anti-climb energy-absorbing device under different thin-walled tube thicknesses. The collision force–displacement curves and energy absorption–displacement curves for different outer tube wall thicknesses are depicted in Figure 5.

From Figure 5a, it can be observed that the variation in the thickness of the thin-walled tube has a significant impact on the initial peak force. The same pattern of influence is observed for the peak force at the second wave crest. For the thin-walled tube with a thickness of 2 mm, the second wave crest differs from those of other thickness parameters, as it begins to decline after only a slight increase. This indicates that changes in the thickness parameter of the thin-walled tube have a considerable effect on the peak force of the anti-climb energy-absorbing device. By reducing the thickness of the thin-walled tube, it is possible to decrease the magnitude of the initial and second wave crest peak forces, thereby reducing the impact force of the collision. At the same time, with the 2 mm thin-walled tube, the displacement difference in the valley peak force between the anti-climb energy-absorbing device and other thicknesses is significant, reaching 59.4 mm. This suggests that reducing the thickness of the thin-walled tube can increase the valley peak force at the front end. The discovery of this phenomenon is of great significance for effectively reducing the

impact peak force and can provide a reference for the orderly crushing design of anti-climb energy-absorbing devices.

From Figure 5b, it is evident that the thickness of the thin-walled tube significantly enhances the energy absorption capacity of the anti-climb energy-absorbing device. When the crushing displacement reaches 538 mm, the device with a 2 mm thin-walled tube absorbs 138 kJ of energy during the collision impact, while the device with a 6 mm thick tube absorbs up to 353 kJ, an increase of 215 kJ, which is a 156% increase compared to the previous value. It also represents a 116% increase compared to the energy absorption of the 5 mm thickness, indicating a significant enhancement effect. In conjunction with Figure 6, it can be seen that although increasing the thickness of the thin-walled tube can significantly improve energy absorption, the peak force also increases accordingly. Therefore, in the design of the anti-climb energy-absorbing device, it is necessary to consider increasing energy absorption while minimizing the impact of the peak force. A possible solution could involve the use of multiple longitudinally arranged induction grooves to reduce the peak force, thus meeting the design requirements of the anti-climb energy-absorbing device.

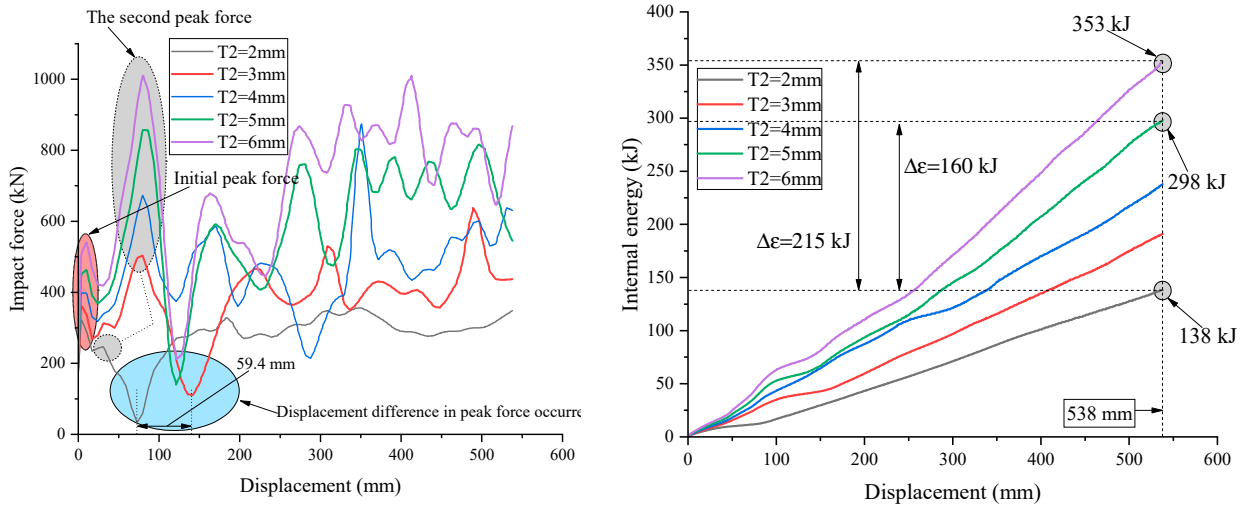


Figure 5. (**a**) Collision force–displacement curves for different outer tube wall thicknesses; (**b**) Influence of thin-walled tube thickness on energy absorption.

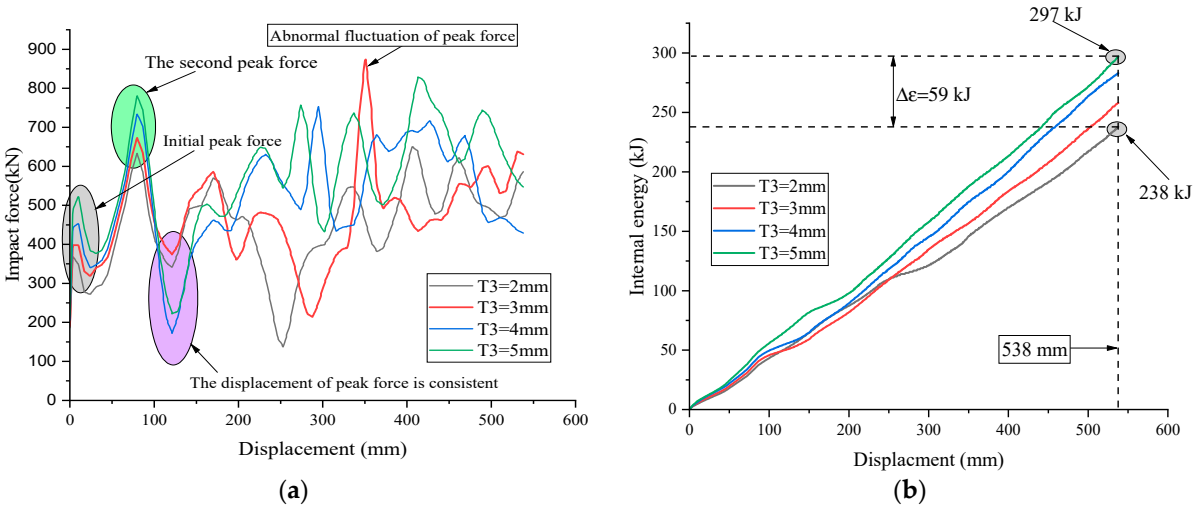


Figure 6. (**a**) Variation in collision force with displacement across different thicknesses of thin-walled inner tubes; (**b**) Variation in energy absorption with displacement across different thicknesses of thin-walled inner tubes.

4.3. Influence of Thin-Walled Inner Tube Thickness

To study the impact of incorporating a thin-walled inner tube on the overall energy absorption performance of the anti-climb energy-absorbing device, a thin-walled inner tube with varying wall thicknesses t_3 of 2, 3, 4, and 5 mm was designed. This thin-walled inner tube is nested on the exterior of the guide beam. The collision force and energy absorption of the anti-climb device were calculated under these different wall thickness conditions. The trends in collision force and energy absorption of the anti-climb energy-absorbing device with varying thin-walled inner tube thicknesses are illustrated in Figure 6.

From Figure 6a, it can be observed that changes in the thickness of both the thin-walled inner and outer tubes exhibit the same trend in collision force variations for both the initial peak force and the second peak force. This suggests that the square thin-walled inner tubes designed for the anti-climb energy-absorbing device have the same load-bearing effect under the impact of a collision. However, unlike the thin-walled outer tubes, the thin-walled inner tubes maintain consistent displacement at the valley peak force, with no significant displacement difference observed across different parameters. Therefore, adjusting the wall thickness of the thin-walled inner tube does not alter the displacement upon which the valley peak force acts, which is distinctly different from the effect of changing the wall thickness parameter of the thin-walled outer tube.

From Figure 6b, it can be seen that as the thickness of the thin-walled inner tube increases, so does its energy absorption capacity. At a displacement of 538 mm, the energy absorption of the anti-climb energy-absorbing device with a 2 mm thick inner tube is 238 kJ, and it increases to 297 kJ with a 5 mm thick inner tube, resulting in an increase of 59 kJ and a 24.8% enhancement in energy absorption. This increase is less pronounced compared to the 116% improvement achieved by increasing the wall thickness of the thin-walled tube by 5 mm. Thus, when the energy absorption of the anti-climb energy-absorbing device is on the lower side and there is a need for enhancement, one can consider increasing the wall thickness of the thin-walled square tubes to improve its energy absorption capacity, while also enhancing the vertical and lateral stiffness of the device.

4.4. Influence of Honeycomb Aluminum Yield Strength

To study the effect of the yield strength of honeycomb materials on the crashworthiness of the anti-climb energy-absorbing device, the yield strength c of the honeycomb aluminum material is selected to be 90, 100, and 110 MPa, respectively. Through finite element simulation calculations, the trends of the collision force and energy absorption of the anti-climb energy-absorbing device with different honeycomb aluminum yield strengths as a function of displacement are obtained and depicted in Figure 7a,b, respectively.

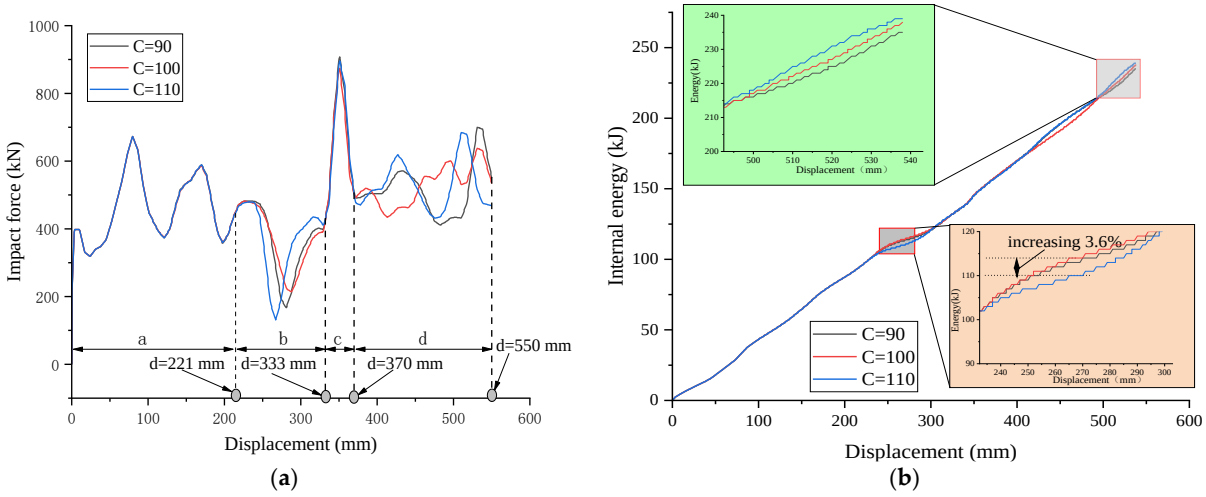


Figure 7. (**a**) Impact of yield strength on impact force; (**b**) Impact of yield strength on energy absorption.

In conjunction with Figure 7b, which illustrates the variation in energy absorption, it can be seen that as the compressive displacement increases, the overall trend of energy absorption for honeycomb aluminum of different strengths remains consistent. However, differences in energy absorption occur within certain compressive displacement ranges, with the energy absorption difference being only 3.6%. This indicates that the yield strength of the embedded honeycomb aluminum is not the primary factor affecting the enhancement of energy absorption in the anti-climb energy-absorbing device.

5. Energy Absorption Effect Optimization

5.1. Experimental Design

The experiment is based on the Latin hypercube sampling (LHS) method, with the honeycomb yield strength c, connecting diaphragm thickness t_1, thin-walled outer tube thickness t_2, and thin-walled inner tube thickness t_3 serving as design variables. The specific energy absorption and peak force F are the design responses. By applying Latin hypercube sampling, combinations of design variables are obtained as shown in Table 2, and the corresponding responses are calculated based on the finite element model.

Table 2. Experimental design matrix.

Sampling	c (MPa)	t_1 (mm)	t_2 (mm)	t_3 (mm)	*SEA* (kJ/kg)	F (kN)
1	106	3	4.17	2.12	15.03	702
2	102	5.17	5.5	2.38	15.15	963
3	104	2	3.5	3.75	15.64	619
4	107	3.5	2.17	2.88	12.91	545
5	109	5	4.67	3.62	15.26	936
6	92	4.83	5.67	3.12	15.74	1050
7	95	4.33	2	2.75	11.81	494
8	96	2.5	4.5	4.62	17.18	862
9	100	4	3.83	3.38	14.98	768
10	90	3.17	3.33	3.5	15.06	710
11	102	4.67	4	5	14.92	844
12	93	5.33	2.83	4.25	13.12	621
13	101	4.17	6	4.12	17.56	1130
14	97	2.33	5.33	3	17.14	976
15	108	2.67	5.83	3.25	18.18	1090
16	91	4.5	5	4.75	15.98	1000
17	107	2.83	5.17	4.88	17.85	1020
18	92	5.83	3.67	2.62	12.28	647
19	97	2.17	2.67	2.5	14.23	464
20	97	2.44	6	3.33	18.26	1140
21	108	4.22	2	4.33	11.61	463
22	103	2	2.89	3	13.93	484
23	90	3.33	3.78	2	12.98	633
24	99	3.78	6	2	16.62	970
25	90	5.56	4.67	3.33	13.22	882
26	101	2.44	3.33	5	15.47	595
27	97	5.11	2.44	4.67	11.52	521
28	110	4.22	2	3.67	11.41	545
29	108	2	4.22	3	15.29	759
30	103	6	3.78	2.33	10.59	602

5.2. Surrogate Model Construction and Evaluation

Response surface models utilize polynomial functions to fit the design space, allowing for a relatively accurate approximation of the actual functional relationships with a limited number of input parameters within a local range.

(1) Surrogate Model Establishment

To establish the mathematical relationship between different parameters and specific energy absorption, as well as to obtain predicted values through input parameters, a second-order response surface method is used to fit 30 experimental samples. The most commonly used polynomial surrogate model is a second-order algebraic polynomial function as follows:

$$\hat{f}(x) = b_0 + \sum_{i=1}^{L} b_i x_i + \sum_{i=1}^{L} b_i x_i^2 + \sum_{i=1}^{L-1} \sum_{j=i+1}^{L} b_{ij} x_i x_j \tag{4}$$

In the formula, $\hat{f}$ represents the approximate response surface function of the true response function f, L is the number of variables in the input vector x, and b_0, b_i, b_{ii}, and b_{ij} are the unknown coefficients that need to be determined using the least squares method.

By approximating the model using a second-order polynomial response surface method, a polynomial surrogate model that characterizes the energy absorption characteristics and crashworthiness of the anti-climb energy-absorbing device, in terms of the specific energy absorption SEA and the maximum peak force F, is obtained as follows:

$$\begin{aligned} SEA = {} & -0.0007c^2 - 0.1707{t_1}^2 - 0.2579{t_3}^2 + 0.0362C * t_2 + 0.1181\ t_1 * t_2 \\ & -2.783t_2 + 2.4174t_3 + 14.6641 \end{aligned} \tag{5}$$

$$\begin{aligned} F = {} & -25.4432{t_1}^2 - 37.49661{t_3}^2 - 10.8294t_1 * t_2 + 16.2734t_2 * t_3 \\ & +250.9143t_1 + 149.2 \end{aligned} \tag{6}$$

(2) Surrogate Model Evaluation

The accuracy of the second-order polynomial surrogate model established based on the design of experiments (DOE) methodology can be assessed using the maximum relative error (MRE), the average relative error (ARE), and the goodness of fit R^2. The goodness of fit is defined as follows:

$$R^2 = 1 - \frac{\sum_{i=1}^{n} (y_i - \hat{y}_i)^2}{\sum_{i=1}^{n} (y_i - \overline{y}_i)^2} \tag{7}$$

The average relative error (AER) is defined as follows:

$$ARE = \frac{\sum_{i=1}^{n} \frac{|y_i - \hat{y}_i|}{y_i} \times 100\%}{n} \tag{8}$$

The maximum relative error (MRE) is defined as follows:

$$MRE = Max \frac{|y_i - \hat{y}_i|}{y_i} \times 100\% \tag{9}$$

In the formula, $\hat{y}_i$ represents the approximate value for the i^{th} sample point, $\overline{y}_i$ is the average value of i sample points, and n is the number of test points. Generally speaking, a surrogate model with a smaller average relative error, a smaller maximum relative error, and a larger goodness of fit (R^2 value closer to 1) indicates the model has a higher accuracy.

A cross-validation of the surrogate models for energy absorption and peak force, established with five random data sample points, was conducted. The accuracy of the obtained surrogate models is presented in Table 3.

Table 3. Error analysis of the response surface model.

Evaluation Index	*SEA*	*F*	Acceptance Level
ARE	0.058	0.038	<0.2
MRE	0.169	0.122	<0.3
R^2	0.923	0.977	>0.9

From Table 3, it can be observed that the accuracy of the surrogate model established based on the response surface method meets the precision requirements of the model in terms of the goodness of fit, average error, and maximum relative error. This indicates that the constructed surrogate model can provide predictions for the energy absorption and the maximum initial peak force of the anti-climb energy-absorbing device.

5.3. Parameter Optimization

A multi-island genetic algorithm is employed to optimize the parameters affecting the specific energy absorption and the maximum initial peak force of the anti-climb energy-absorbing device. With the specific energy absorption *SEA* and the peak force *F* as the optimization objectives, the honeycomb aluminum yield strength c, connecting diaphragm thickness t_1, thin-walled outer tube thickness t_2, and thin-walled inner tube thickness t_3 are considered as design variables. The optimization problem regarding the anti-climb energy-absorbing device's influencing parameters is defined as follows:

$$\begin{cases} Maximize : SEA \\ Minimize : F \\ Subject : X^L \leq X \leq X^M \end{cases} \tag{10}$$

In the formula, $X = [c, t_1, t_2, t_3]$ represents the design variables of the optimization model (mm), $X^L = [{x_1}^l, {x_2}^l, {x_3}^l, {x_4}^l]$ represents the lower bounds, and $X^M = [{x_1}^m, {x_2}^m, {x_3}^m, {x_4}^m]$ represents the upper bounds for the four design variables. The constraint boundary conditions are $t_1 \in [2,6]$, $t_2 \in [2,6]$, $t_3 \in [2,5]$, $c \in [90,110]$.

The optimization results for the specific energy absorption and maximum peak force of the anti-climb energy-absorbing device, obtained using the multi-island genetic algorithm, are presented in Table 4. The predicted results from the surrogate model established by the response surface method are compared with the actual values in Table 5.

Table 4. Comparison of optimization results.

	Parameter				Crashworthiness		
	c (MPa)	t_1 (mm)	t_2 (mm)	t_3 (mm)	*SEA* (kJ/kg)	*F* (kN)	*Q* (kJ)
Initial parameter	100	4	4	2	14.5	880	238
Optimized result	104	2.5	4.5	5	16.5	939	303
Effect after optimization	/		/	/	+13.8%	6.7%	27.3%

Table 5. Verification of prediction results.

Comparison	c (MPa)	t_1 (mm)	t_2 (mm)	t_3 (mm)	*SEA* (kJ/kg)	*F* (kN)	*RE* (SEA)	*RE* (*F*)
True value	104	2.5	4.5	5	16.5	939	2.5%	9.9%
Predicted value	104	2.5	4.5	5	16.9125	846		

From Table 4, it can be seen that the maximum relative errors between the predicted values and the actual values for the specific energy absorption and the maximum peak force of the anti-climb energy-absorbing device, as established by the response surface method, are 2.5% and 9.9%, respectively. These error values are both less than 10%, indicating that the established surrogate model meets the computational requirements and possesses a

satisfactory predictive capability. Using the surrogate model in conjunction with a multi-island genetic algorithm to optimize the initial structure of the anti-climb energy-absorbing device, the optimized parameters obtained, such as the connecting diaphragm thickness, thin-walled outer tube thickness, thin-walled inner tube thickness, and the yield strength of the aluminum honeycomb, result in an energy absorption of 303 kJ and a maximum peak force of 939 kN. This represents an increase of 27.3% in energy absorption and 13.8% in specific energy absorption, with only a 6.7% increase in the maximum peak force, achieving the goal of absorbing more energy while keeping the initial peak force as low as possible. To verify the accuracy of the optimization results (Table 4), our finite element simulation calculations yielded energy absorption and maximum peak force values of 58.2 J and 4.16 kN, respectively, with the maximum relative errors between the optimized predicted values and the actual values being 2.5% and 9.9%. This demonstrates that the optimization results obtained using the genetic algorithm meet the accuracy requirements and can be used for the optimized design of the energy absorption and maximum impact load parameters of the anti-climb energy-absorbing device.

Our study of the crashworthiness of the anti-climb energy-absorbing device using a combined method of the polynomial response surface and the multi-island genetic algorithm indicates significant optimization effects in terms of the specific energy absorption and energy absorption of the device. This research method provides valuable references for the application of anti-climb energy-absorbing devices in engineering.

6. Conclusions

In this paper, a novel double-layer square tube composite anti-climb energy-absorbing device filled with honeycomb aluminum blocks was designed. A collision finite element model was established using LS-DYNA to study the impact of different connecting diaphragm thicknesses, thin-walled outer tubes, thin-walled inner tubes, and yield strengths of the honeycomb aluminum on the crashworthiness of the anti-climb energy-absorbing device. Furthermore, with the specific energy absorption and peak force as the optimization objectives, the response surface method and a multi-island genetic algorithm were employed to identify the optimal wall thickness combinations within the design space, leading to the following conclusions:

(1) Regarding the influence of the connecting diaphragm thickness, thin-walled inner and outer tubes, and yield strength of the honeycomb aluminum on the crashworthiness of the anti-climb energy-absorbing device, the connecting diaphragm thickness and the yield strength of the honeycomb aluminum have a relatively minor impact on energy absorption. The connecting diaphragm thickness has a more pronounced effect on the maximum peak force, while the thickness of the thin-walled tubes significantly affects both the energy absorption and the maximum peak force.

(2) The polynomial surrogate model established based on the response surface method can effectively predict the energy absorption and maximum peak force of the anti-climb energy-absorbing device under collision impact, providing a reference for structural crashworthiness research in the field of engineering.

(3) An optimization analysis was conducted on the influencing factors of the anti-climb energy-absorbing device, such as the connecting diaphragm thickness, thin-walled outer tube thickness, thin-walled inner tube thickness, and yield strength of the honeycomb aluminum, using a multi-island genetic algorithm. The optimization was significant, with the optimized structural parameters leading to a substantial increase in energy absorption and specific energy absorption, while the maximum peak force increased by only 6.7%.

Author Contributions: Conceptualization, S.X., T.Z. and L.X.; Methodology, Y.L.; validation, H.Z.; Investigation, J.X. and G.Z.; Writing—original draft preparation, Y.L.; Writing—review and editing, Y.L.; funding acquisition, S.X., T.Z. and Y.L. All authors have read and agreed to the published version of the manuscript.

Funding: This research was funded by the National Natural Science Foundation Project of China (grant numbers 52175123 and 52172409), by Key Technologies R&D Program of Henan Province (grant number 232102240092), by Heilongjiang Province Postdoctoral Foundation Project (grant number LBH-Z23041), and by the 2023 Special Project for the Cultivation of Original Technology Decade (grant number 2022CYY007).

Institutional Review Board Statement: Not applicable.

Informed Consent Statement: Not applicable.

Data Availability Statement: The raw data supporting the conclusions of this article will be made available by the authors on request.

Acknowledgments: Thanks to Xiangwei Li for funding the project (2022CYY007) and their support of this paper.

Conflicts of Interest: Author Yuru Li was employed by the company CRRC Qiqihar Rolling Stock Co., Ltd. The remaining authors declare that the re-search was conducted in the absence of any commercial or financial relationships that could be construed as a potential conflict of interest.

References

1. Zhou, H.; Mei, M.; Zhang, J.; Tu, H. Investigations on the vertical buckling of railway vehicle's anti-climber. *Int. J. Crashworthiness* **2021**, *26*, 171–181. [CrossRef]
2. Zhou, H.C.; Bao, Z.Y.; Xu, S.Z.; Zhang, J.M.; Tu, H.Y. Study on the Vertical Buckling of Railway Vehicle's Anti-climber. *J. Mech. Eng.* **2019**, *55*, 170–175.
3. Gao, G.; Guan, W.; Li, J.; Dong, H.; Zou, X.; Chen, W. Experimental investigation of an active-passive integration energy absorber for railway vehicles. *Thin-Walled Struct.* **2017**, *117*, 89–97. [CrossRef]
4. Jiang, S.H. Crash simulation and experimental verification of the train anti-climber. *Chin. J. Constr. Mach.* **2018**, *16*, 274–277+282.
5. Peng, Y.; Deng, W.; Xu, P.; Yao, S. Study on the collision performance of a composite energy-absorbing structure for subway vehicles. *Thin-Walled Struct.* **2015**, *94*, 663–672. [CrossRef]
6. Gao, G.; Shu, K.; Guan, W.; Yu, Y. Crashworthiness analysis of shrinking circular tube energy absorbers with an anti-clamber for trains. *J. Railw. Sci. Eng.* **2022**, *19*, 520–527.
7. Yin, H.; Wen, G.; Liu, Z.; Qing, Q. Crashworthiness optimization design for foam-filled multi-cell thin-walled structures. *Thin-Walled Struct.* **2014**, *75*, 8–17. [CrossRef]
8. Zhang, Z.; Liu, S.; Tang, Z. Crashworthiness investigation of kagome honeycomb sandwich cylindrical column under axial crushing loads. *Thin-Walled Struct.* **2010**, *48*, 9–18. [CrossRef]
9. Yao, S.; Xiao, X.; Xu, P.; Qu, Q.; Che, Q. The impact performance of honeycomb-filled structures under eccentric loading for subway vehicles. *Thin-Walled Struct.* **2018**, *123*, 360–370. [CrossRef]
10. Forsberg, J.; Nilsson, L. Evaluation of response surface methodologies used in crashworthiness optimization. *Int. J. Impact Eng.* **2006**, *32*, 759–777. [CrossRef]
11. Ihsan, M.N.; Santosa, S.P.; Gunawan, L.; Budiwantoro, B. Design and optimization of anti-climber device for light rail transit crash energy management system. *Int. J. Crashworthiness* **2022**, *28*, 664–675. [CrossRef]
12. Chen, S.; Niu, W.; Wen, T. Simulation of Urban Rail Vehicle Crash and Factors Influencing Anti-climbing Ability of its Anti-climber. *J. Mech. Strength* **2015**, *37*, 924–929.
13. Djamaluddin, F.; Abdullah, S.; Ariffin, A.K.; Nopiah, Z.M. Finite element analysis and crashworthiness optimization of foam-filled double circular under oblique loading. *Lat. Am. J. Solids Struct.* **2016**, *13*, 2176–2189. [CrossRef]
14. Yildiz, A.R.; Solanki, K.N. Multi-objective optimization of vehicle crashworthiness using a new particle swarm-based approach. *Int. J. Adv. Manuf. Technol.* **2012**, *59*, 367–376. [CrossRef]
15. Yin, H.; Wen, G.; Hou, S.; Qing, Q. Multiobjective crashworthiness optimization of functionally lateral graded foam-filled tubes. *Mater. Des.* **2013**, *44*, 414–428. [CrossRef]
16. Marzbanrad, J.; Ebrahimi, M.R. Multi-objective optimization of aluminum hollow tubes for vehicle crash energy absorption using a genetic algorithm and neural networks. *Thin-Walled Struct.* **2011**, *49*, 1605–1615. [CrossRef]
17. Zheng, X.; Zhong, J.; Sun, Y.; Shi, Y.; Xu, Z.; Sun, H. Design of Optimization Platform for Energy Absorption Structure of High-Speed Train. In Proceedings of the 2019 IEEE 23rd International Conference on Computer Supported Cooperative Work in Design (CSCWD), Porto, Portugal, 6–8 May 2019; pp. 279–283.
18. Li, Y.R.; Zhu, T.; Xiao, S.N.; Yang, B.; Yang, G.W.; Yuan, X.L.; Tang, Z. Application of Collision Mathematical Model Based on BP Neural Network in Railway Vehicle. *Proc. Inst. Mech. Eng. Part F J. Rail Rapid Transit* **2020**, *235*, 713–725. [CrossRef]
19. Li, Y.R.; Zhu, T.; Tang, Z.; Xiao, S.N.; Xie, J.K.; Liu, Z.B.; Xiao, S.D. Inversion prediction of back propagation neural network in collision analysis of anti-climbing device. *Adv. Mech. Eng.* **2020**, *12*, 1687814020922050. [CrossRef]

20. Xu, P.; Yang, L.; Yao, S.; Guo, W.; Che, Q.; Wang, A. Collision mechanics parameter design and multi-objective optimization of square cone anti-climbing energy-absorbing structure for urban rail trains. *J. Cent. South Univ.* **2022**, *53*, 1689–1699.
21. *EN 15227*; Railway Applications—Crashworthiness Requirements for Rail Vehicles. European Standard: Plzen, Czech Republic, 2020.

Disclaimer/Publisher's Note: The statements, opinions and data contained in all publications are solely those of the individual author(s) and contributor(s) and not of MDPI and/or the editor(s). MDPI and/or the editor(s) disclaim responsibility for any injury to people or property resulting from any ideas, methods, instructions or products referred to in the content.